European Journal of Pharmaceutical Sciences 174 (2022) 106207

Contents lists available at ScienceDirect

European Journal of Pharmaceutical Sciences

journal homepage: www.elsevier.com/locate/ejps

Ultrasound responsive Gd-DOTA/doxorubicin-loaded nanodroplet as a theranostic agent for magnetic resonance image-guided controlled release drug delivery of melanoma cancer

Fatemeh Maghsoudinia [a], Hadi Akbari-Zadeh [b,c], Fahimeh Aminolroayaei [d], Fariba Farhadi Birgani [e], Ahmad Shanei [d,*], Roghayeh Kamran Samani [f,*]

[a] Department of Medical Imaging and Radiation Sciences, Faculty of Paramedicine, Ahvaz Jundishapur University of Medical Sciences, Ahvaz, Iran
[b] Department of Medical Physics, Faculty of Medicine, Mashhad University of Medical Sciences, Mashhad, Iran
[c] Student Research Committee, Mashhad University of Medical Sciences, Mashhad, Iran
[d] Department of Medical Physics, School of Medicine, Isfahan University of Medical Sciences, Isfahan, Iran
[e] Department of Radiology, Shoushtar Faculty of Medical Sciences, Shoushtar, Iran
[f] Department of Medical Physics and Radiology, School of Allied Medical Sciences, Shahrekord University of Medical Sciences, Shahrekord, Iran

ARTICLE INFO

Keywords:
Ultrasound responsive nanodroplets
Gd-DOTA (Dotarem)
Doxorubicin
Controlled release drug delivery
Image-guided cancer therapy
Melanoma cancer

ABSTRACT

Theranostic agents use simultaneous for diagnostic and therapeutic procedures. In the present study, the effect of Gd-DOTA/doxorubicin-loaded perfluorohexane nanodroplets as a theranostic nanoparticle for control released drug delivery and ultrasound/MR imaging was investigated on B16F10 melanoma cancer cells. The intracellular uptake was performed by inductively coupled plasma optical emission spectrometry (ICP-OES) that indicated sonicated Gd-DOTA/DOX@PFH NDs uptake by cancer cells was approximately 1.5 times more than the non-sonicated nanodroplets after 12 h. *In vitro* and *in vivo* toxicity assays revealed that synthesized NDs are biocompatible and do not have organ toxicity. Ultrasound exposure significantly enhanced the release of doxorubicin from NDs (P-value< 0.05). Ultrasound echogenicity and T_1-MRI relaxometry indicated that synthesized NDs have strong ultrasound signal intensity and high r_1 relaxivity (6.34 mM^{-1} S^{-1}). The concentration of DOX in mice vital organs for Gd-DOTA/DOX NDs was significantly lower than that of free DOX. Doxorubicin concentration after 150 min in the tumor region for the DOX-loaded Gd-NDs+US group reached 14.8 μg/g followed by sonication, which was 2.3 fold higher than that of the non-sonicated group. According to the obtained results, the synthesized nanodroplets, with excellent diagnostic (ultrasound/MRI) and therapeutic properties, could be promising theranostic agents in cancer imaging and drug delivery for chemotherapeutic application.

1. Introduction

Cancer diagnosis is crucial for its effective treatment (Guo et al., 2016). In recent years, many efforts have been made to develop new methods for the cancer diagnosis and treatment. Conventional diagnostic and therapeutic methods, despite all the human assistance, restricted with serious limitations such as the delay between diagnosis and treatment, side effects, inability to track therapeutic agents to reach in the desired area and targeted treatments (Palekar-Shanbhag et al., 2013). However, recent advances in various sciences promise to overcome these limitations (Jeyamogan et al., 2021). Theranostic is one of these promising aspects which studies the simultaneous use of therapeutic and diagnostic agents in one system (Rammohan et al., 2016; Zhu et al., 2015).

Nanotechnology is a branch of science that has attracted the attention of many researchers (Shanei et al., 2019). Today, nanotechnology plays an undeniable role in many scientific fields which one of them is theranostic (Chiari-Andréo et al., 2020). Various studies have shown that nanomaterials have the ability to improve treatment efficiency and even by using their power, several goals can be pursued simultaneously (Maghsoudinia et al., 2021).

Magnetic resonance imaging (MRI) is one of the most important, widely used, and powerful imaging modalities (Fasano et al., 2018). MRI uses in different medical aspects such as diagnosis, treatment,

* Corresponding authors.
E-mail addresses: shanei@med.mui.ac.ir (A. Shanei), kamran.r@skums.ac.ir (R.K. Samani).

https://doi.org/10.1016/j.ejps.2022.106207
Received 7 December 2021; Received in revised form 8 May 2022; Accepted 11 May 2022
Available online 13 May 2022

following-up, and treatment evaluation. This method can provide high spatial resolution without penetration tissue depth limit, no ionizing radiation, multi-planar imaging, and function of soft tissues (Maghsoudinia et al., 2021). Gadolinium (Gd) is the most widely used contrast agent in MRI due to its individual magnetic property (Kim et al., 2018). This agent is used in nearly half of MRI scans (Xiao et al., 2016) and helps to see inflammation, infection, tumors, and blood vessels better in the specific organs (Lazaro-Carrillo et al., 2020). However, the free ions of Gd (Gd^{+3}) are very toxic and deposition of them in the body leads to biological toxicity (Ranga et al., 2017). Chelate ligand complexes such as Dotarem (Gd-DOTA) are used in order to reduce the metal ions toxicity but there are concerns about the release of Gd ions and their harmful consequences (Xiao et al., 2016). Using nanotechnology and loading Gd ions in nanocarriers can be considered as a solution to reduce their toxicity (Shafaei et al., 2019).

Doxorubicin (DOX) is a widely prescribed chemotherapeutic drug used for cancer treatments (Franco et al., 2018). Despite all its anti-tumor properties, it causes toxicity and damage to the brain, heart, liver, and kidneys (Carvalho et al., 2009). A controlled release drug delivery is used due to bring the maximum agent to the desired area and minimize its uptake by the other tissues. With this approach, treatment efficiency can be increased and drug side effects can be reduced (Bhowmik et al., 2012). One of the controlled release drug methods is using ultrasound (US) waves and gas-encapsulated microbubbles (MBs) (Huang et al., 2021). The MBs cavitation induced by US waves leads to drug release and increases permeability in target tissues (Wang et al., 2013). While MBs are currently used as contrast agents in the US imaging, however, their relatively large size, poor stability, and short circulation time limited their use (Wang et al., 2013; Yoon et al., 2017). There are nanodroplets (NDs) that sensitive structures to ultrasound waves and change their phase when exposed to US waves. The core of NDs is usually made of fluorocarbon such as perfluorohexane (PFH) which is in the liquid phase at body temperature. The NDs don't have MBs limitation and their nucleus evaporates to MBs after US exposure with sufficient pressure (Maghsoudinia et al., 2021). This phenomenon is called the acoustic droplet vaporization (ADV) effect (Loskutova et al., 2019). The drug can be released into the target tissue due to volumetric expansion of NDs and the formation of acoustically active MBs (Sheeran and Dayton, 2012). In addition, these events produce high acoustic signals that can be used for US imaging (Maghsoudinia et al., 2021).

Coating nanoparticles with safe biopolymers can reduce their toxicity and increase their biocompatibility (Pinelli et al., 2020). Polysaccharide alginate is a polymer that, in addition to the stated advantages, has a relatively low price, available, and biodegradable (Shafaei et al., 2019).

The aim of this study is to investigate the theranostic agent of Gd-DOTA/DOX@PFH NDs coated with polysaccharide alginate as a dual contrast agent in US/MR imaging and drug delivery systems. These NDs with controlled drug delivery capability can be release doxorubicin after ensuring the drug accumulation in the target tissue using monitoring with US/MR imaging.

2. Materials and methods

2.1. Materials

Sodium alginate, perfluorohexane (PFH), Dimethyl Sulfoxide (DMSO), and Cell proliferation kit (MTT) were purchased from Sigma-Aldrich (Germany). Tween 20 was obtained from Merck (Germany). Fetal Bovine Serum (FBS) was purchased from Gibco (Australia). Phosphate-Buffered Saline (PBS), and trypsin were obtained from Sigma-Aldrich (USA). Dotarem (Gd-DOTA) was purchased from Guerbet (France). Melanoma cancer (B16F10), and normal fibroblast (L929) cell lines were obtained from the Pasteur Institute, Iran.

2.2. Synthesis of Gd-DOTA/doxorobicin-loaded nanodroplets

In this study, the emulsion synthesis method was used to prepare nanodroplets. At this stage, initially, PFH (500 μL) in distilled deionized water (2 mL) was homogenized at 24000 rpm for 2 min using a homogenizer (Ultra-Turrax SG215, Staufen, Germany) in an ice bath. Afterward, Gd-DOTA (Dotarem, 0.5 mmol mL^{-1}, 1 mL) and surfactant (Tween 20, 10 μL) were added to the solution, and it was homogenized at 17000 rpm for 2 min. Then, alginate polysaccharide (1.5% w/v) was added to the solution under homogenizing 13000 rpm for 3 min for the preparation of Gd-DOTA/DOX@PFH NDs. After that, $CaCl_2$ (0.2 w/v) solution was added and homogenized at 3000 rpm for 3 min. After stirring for 2 h, the solution was centrifuged for 30 min at 11000 rpm at 4 °C. Finally, the supernatant was aspirated and the obtained nanodroplets were dispersed in PBS (5 mL) and stored at 4 °C.

2.3. Physicochemical characterization

Transmission electron microscopy (TEM) images were captured using transmission electron microscopy ((Philips em208s, Netherlands)) at voltage of 100 kV. Hydrodynamic diameter sizes were measured by dynamic light scattering (DLS) with Vascov/Cordouan Technologies (France). Magnetic characterization was performed by Vibrating Sample Magnetometer (VSM, MDKB, Meghnatis Daghigh Kavir, Iran) at 300 °K. Concentration of the Gd^{3+} ions in all prepared NDs suspensions was measured using an inductively coupled plasma optical emission spectrometer (ICP-OES, Varian Vista-Pro, Australia) by dissolving samples in aqua regia (hydrochloric acid/nitric acid mixture). To determine the amount of drug encapsulation after centrifugation of nanodroplets emulsion for 30 min at 11000 rpm, the supernatant was collected and the drug amount in the supernatant was determined using the UV-Vis spectrophotometer. Then the percentage of drug loading efficiency in nanoparticle structure was calculated according to Eq. (1):

$$\text{Percentage of drug loading efficiency} = \frac{(\text{Total amount of drug added}) - (\text{Free amount of drug})}{\text{Total amount of drug added}} \times 100 \quad (1)$$

To test the stability of NDs, the emulsion was kept at 4 ∘C for 3 months, and the size of the nanoparticles and entrapment efficiency were determined every 15 days using DLS and UV-Vis, respectively.

2.4. Passive and active drug release

To evaluate passive drug release, 10 mL of phosphate buffer for pH 7.4, and acetate buffer for pH 5.5 were poured in two different jars and 10 mg Gd-DOTA/DOX NDs per each jar were dispersed in them. Then, the dispersion was divided into five equal aliquots (2 mL). Each sample was transferred into a dialysis bag (molecular weight cut off=12,000) and immersed in 80 mL of different buffers (pH = 7.4 and 5.5) and shaken at 200 rpm and 37 °C in a shaker incubator. 3 mL of the solution was obtained at defined intervals (2, 6, 12, 24, and 36 h), from the reservoir, and the amount of released DOX was measured by UV–Vis at 498 nm.

To assess the active drug release profiles, the drug-loaded

nanodroplets were poured into a latex finger cot which was immersed in a large tank containing PBS at 37 °C. The ultrasound at the frequency of 1 MHz and 1.5 W cm^{-2} was applied to expose samples at predetermined intervals (0, 2, 4, 6, 8 and, 10 min). Afterwards, 1 mL of the nanodroplets solution was taken out and centrifuged at 11000 rpm. The DOX concentrations in the supernatant were determined using UV-Vis spectrometry.

2.5. Assessment of ADV effect by ultrasound imaging

To monitor the ADV effect and formation of microbubbles from nanodroplets, ultrasound imaging of PBS (as control solution) and synthesized NDs was carried out by a B-mode diagnostic ultrasound imaging system (UGEO H60, Samsung). The images were captured with a mechanical index (MI) of 1.4 before and after the NDs injection into the PBS. To avoid air background, the probe was coated with ultrasound gel.

2.6. Relaxivitiy study

Samples (Gd-DOTA and Gd-DOTA/DOX-loaded NDs) were diluted in distilled water at various Gd concentrations (0, 0.05, 0.1, 0.2, 0.4, 0.6, 0.8 and 1 mM). Relaxivity experiments were carried out by recording T_1 map with a 1.5 T MR imaging scanner (Magnetom Aera, Siemens, Germany) with the following T_1-weighted imaging parameters: repetition time (TR) =150, 300, 500, 700, 900, 1200, and 2000 ms, echo time (TE) = 9 ms, fields of view (FOV) = 192 × 220 mm^2, matrix size = 224 × 320, slice thickness = 3 mm, and flip angle = 90°. The obtained data were analyzed by MATLAB 9.4 software (MathWorks, Natick, MA, USA). Relaxivity values of samples (r_1) were obtained from the slope of the relaxation time (1/T1) versus Gd^{3+} concentration.

2.7. Cell culture

B16F10 melanoma cancer and L929 normal cells were grown in high-glucose Dulbecco's Modified Eagle Medium (DMEM) supplemented with 10% FBS, 1% penicillin/streptomycin, and then were maintained at 37 °C with 5% CO_2.

2.8. Cytotoxicity assay

MTT test was performed for evaluating the cytotoxicity and biocompatibility of nanoparticles with and without ultrasound. Also, cell viability was assessed for ultrasound exposure alone. The cytotoxicity at different DOX concentrations (0.05, 0.1, 25, 0.5, 1, and 2 μg mL^{-1}) was evaluated and the optimal concentration was selected for future studies. For sonication groups, 1 h after NPs treatments, the cells were sonicated by a 1 MHz ultrasound probe and the MTT assay was performed after 23 h. To assess the cell viability, the topsoil of the cells was discarded and 100 μL of medium containing 0.5 mg mL^{-1} of MTT was added to each well and then incubated for 4 h. Afterward, the top liquid was removed and 100 mL of DMSO was added to each well to dissolve the formazan crystals. Finally, the light absorption of each well was read using an ELISA device at a wavelength of 570 nm.

2.9. Cellular uptake of nanodroplets

To evaluate the cellular uptake of NDs, 2 × 10^6 of B16F10 cancer cells were seeded into each well of a 6-well culture plate and then incubated for 24 h. Then the cells were incubated with Gd-DOTA/DOX-loaded NDs at 50 μg mL^{-1} Gd concentration (with and without sonication) for 0.5, 3, 6, and 12 h at 37 °C with 5% CO_2. Afterward, the cells were washed with PBS, detached via trypsin, centrifuged at 1500 rpm for 5 min, reconstituted in 100 μL of PBS, and dissolved in 3 mL of aqua regia. Intracellular uptake of Gd^{3+} ions was quantified by ICP-OES. The average uptake amount of Gd^{3+} ions by each B16F10 cell was determined based on the total number of cells and measured Gd^{3+} concentration. The assessments were carried out in triplicate and the mean value ± standard deviation (SD) of obtained results were calculated.

2.10. MRI

B16F10 cells (3 × 10^6 cells in each group) were incubated with Gd-DOTA and Gd-DOTA/DOX NDs at various Gd concentrations (0, 0.2, 0.4, 0.6, 0.8 and 1 mM) for 6 h at 37 °C. Distilled water was used as the control solution. After incubation time, the cells were washed with PBS, detached by adding trypsin, collected the following centrifugation, and transferred into microtubes containing 2% agarose gel. Following solidification of agarose gel, contrast-enhanced MR images of cells were obtained by a 1.5 T MRI system. Parameters used for the T_1-weighted imaging were: TR=500 ms, TE=11 ms, matrix size= 224 × 320, slice thickness =3 mm, flip angle=90°, and FOV=192 × 220 mm^2. Finally, all MRI data were analyzed by MATLAB 9.4 software.

2.11. Hemolysis assay

Hemocompatibility of free DOX and Gd-DOTA/DOX-loaded nanodroplets was assessed *in vitro*. The fresh human blood was collected and centrifuged at 1500 rpm for 15 min to harvest the human red blood cells (HRBCs). Then, they were refined using consecutive rinsing with PBS buffer (pH 7.4). Afterward, the HRBCs suspension was diluted ten times, and then 200 μL of HRBCs suspension was added to 800 μL of each sample with different DOX concentrations (10–200 μg mL^{-1}). In this study the PBS buffer (pH 7.4) and Triton X-100 (2% v/v) were used as negative and positive controls, respectively. After 2 h, the prepared samples were centrifuged at 11000 rpm for 30 min at 4 °C. The absorbance value (Abs) of the collected supernatant was measured by UV–Vis spectrophotometer at 540 nm. The hemolysis percentage of each sample was calculated using the following equation:

$$\text{Hemolysis}\% = \frac{(Abs_{Sample} - Abs_{Ctrl-})}{(Abs_{Ctrl+} - Abs_{Ctrl-})} \times 100 \quad (2)$$

2.12. In vivo biocompatibility of the Gd-DOTA/DOX nanodroplets

For evaluating blood biochemistry and organ toxicity of synthesized Gd-DOTA/DOX NDs, the normal C57BL/6 mice were injected with 2 mg kg^{-1} DOX of Gd-DOTA/DOX NDs. The mice with the injection of PBS were used as a control group. The animals were sacrificed 20 days after administration. Then, their blood was collected for hematology analysis, and their vital organs were harvested for the histopathological exam. The white blood cells (WBC), red blood cells (RBC), platelets (PLT), and hemoglobin (HGB), were measured for hematological assays. Also, creatinine (Cr), blood urea nitrogen (BUN), aspartate aminotransferase (AST), alanine aminotransferase (ALT), total bilirubin (TB), total protein (TP), globulin (GLOB), and albumin (ALB), were measured as biochemical examinations. In addition, different harvested organs including liver, kidneys, brain, lung, heart, and spleen were fixed in 4% formaldehyde and embedded in paraffin. Then, after dehydration of organs, the tissues were blocked. In the next step, thin sections (5 μm) of each organ were prepared and then stained by hematoxylin and eosin. Histological photographs of organs were captured by a digital light microscope (Olympus, Japan).

2.13. In vivo biodistribution of DOX and NDs

Three groups of melanoma tumor-bearing C57BL/6 mice including free DOX, Gd-DOTA/DOX NDs, and Gd-DOTA/DOX NDs followed by ultrasound exposure (1 MHz for 4 min) were considered for this test. In the third group, the tumor site 150 min after injection of Gd-DOTA/DOX NDs was exposed with ultrasound waves for 5 min. The ultrasonic gel was used as a coupling layer between the tumor surface and the

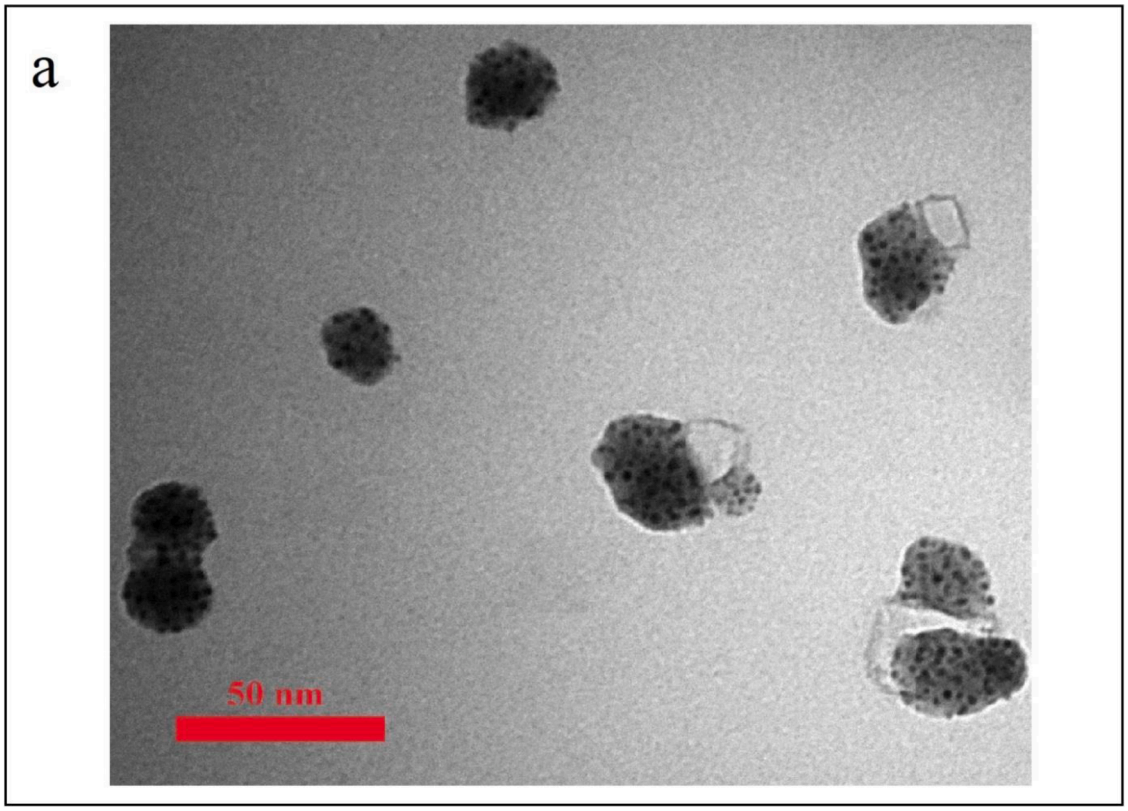

b

Days	0	15	30	45	60	75	90
Particle size (nm)	37.1±2.1	37.8±3.2	38.5±2.5	38.8±3.3	39.1±3.4	40.2±2.8	40.6±3.1
Entrapment efficiency (%)	92.11%	91.45%	91.11%	90.91%	90.01%	89.71%	89.12%

Fig. 1. (a) The TEM image of Gd-DOTA/DOX-loaded NDs. (b) Stability evaluation of Gd-DOTA/DOX NDs by assessing the changes in their sizes by DLS and entrapment efficiency of doxurobicine in nanodroplets after storage at 4 ℃ for 3 months.

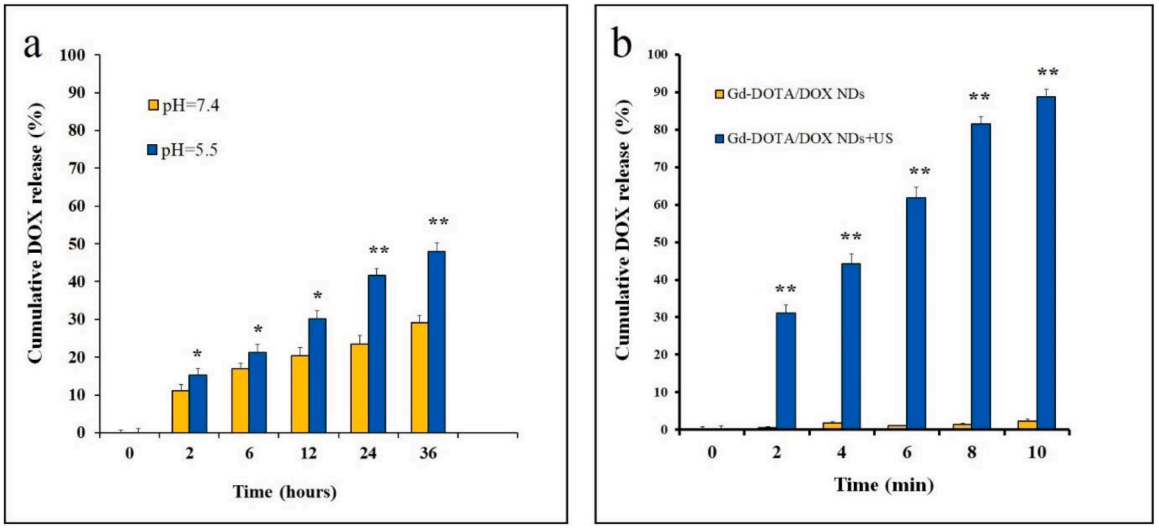

Fig. 2. (a) The Passive release profile of DOX from PFH nanodroplets at normal (7.4) and acidic pH (5.5). (b) The active release profile of DOX from NDs after ultrasound exposure (1 MHz, 1.5 W cm^{-2}) in pH 7.4, at 37 °C. Means ± SD ($n = 3$). * P-value< 0.05; ** P-value < 0.01.

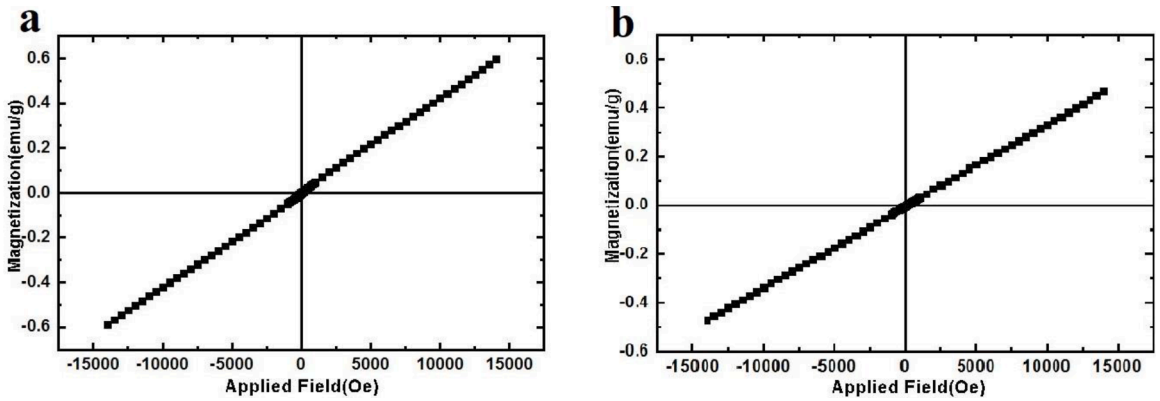

Fig. 3. VSM analyzes of (a) Gd-DOTA, and (b) Gd-DOTA/DOX NDs (magnetization (emu g^{-1}) as a function of applied fields (Oe)) at room temperature.

ultrasound probe. The injection concentration in all groups was 2 mg DOX/kg mice's body weight.

2.14. Blood circulation time

To measurement the blood circulation time, the C57BL/6 mice ($n = 3$ per group) were injected with 2 mg DOX/kg mice's body weight of free DOX and Gd-DOTA/DOX NDs. After different time intervals (10 30 min, 3, 6, 12, and 24 h), the blood samples (0.5 mL) were collected via the cardiac puncture. Then the samples were dissolved in Ethanol / hydrochloric acid mixture and centrifuged. The drug concentration in the supernatant was measured using a UV-Vis spectrophotometer. To evaluation of the distribution phase of DOX, the relationship between the log concentration of drugs and time was assessed. DOX pharmacokinetic parameters in mouse serum after IV injection of free DOX and DOX-loaded NDs were obtained.

2.15. Statistical analysis

In this study, obtained data were processed with SPSS software and expressed as the mean ± standard deviation (SD). The plots showed with error bars which indicated the standard deviation (error) of the mean. Statistical analysis was performed using the one-way ANOVA according post-hoc Tukey's multiple comparison test. In statistical comparisons, *P*-value > 0.05 and *P*-value < 0.05 were taken as indicators of statistically insignificant and significant differences, respectively.

3. Results and discussion

3.1. Synthesis and evaluation of nanodroplets properties

In this study, Gd-loaded NDs containing doxorubicin were prepared using a nano-emulsion method. The mean hydrodynamic size of Gd-DOTA/DOX NDs in DLS analysis was 37.1 ± 3.2 nm. In addition, as

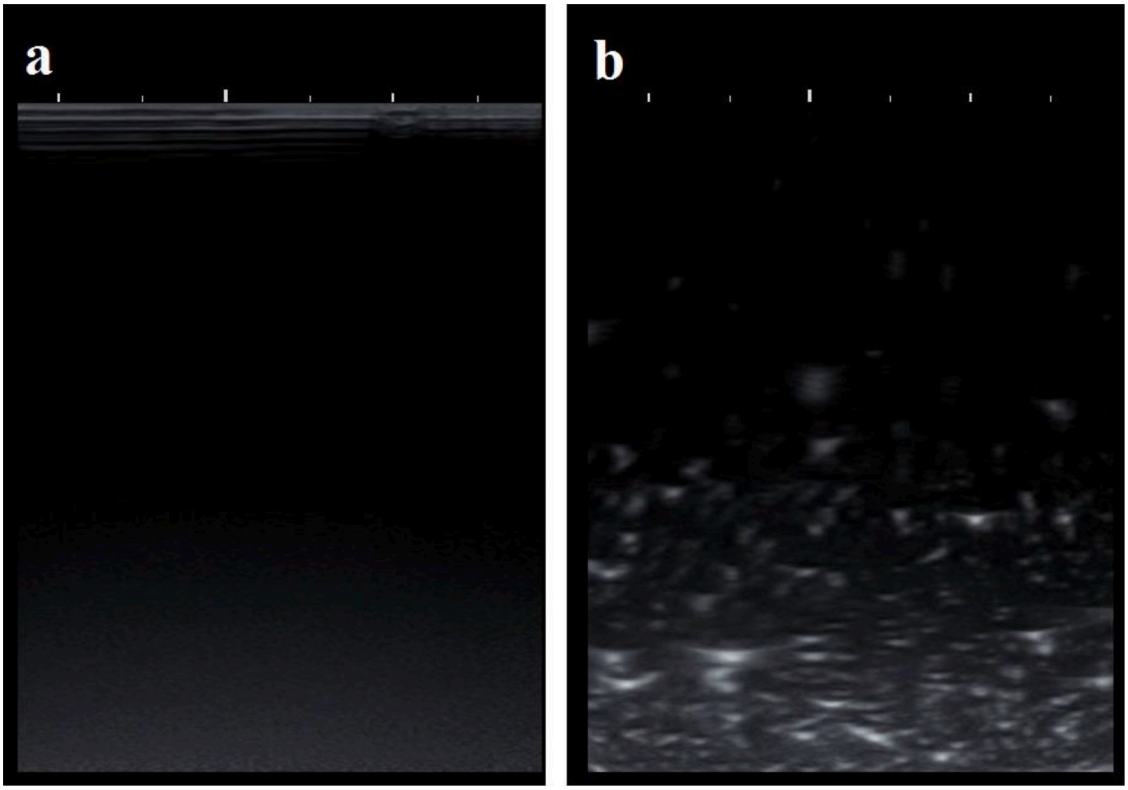

Fig. 4. Ultrasound imaging of (a) PBS (control), and (b) Gd-DOTA/DOX NDs after injection into PBS.

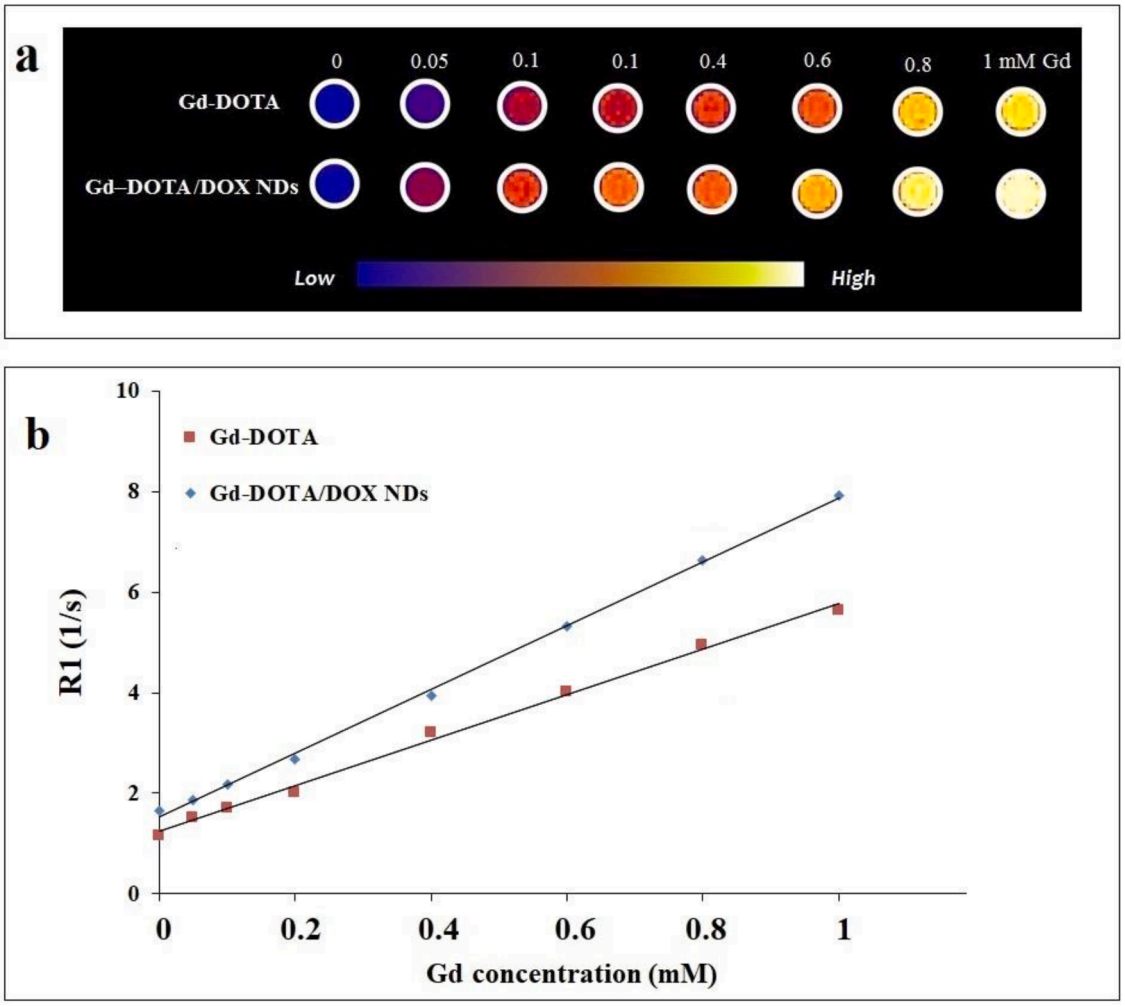

Fig. 5. (a) T_1-weighted MRI images and (b) r_1 relaxivity plots of Gd-DOTA, and Gd-DOTA/DOX-loaded NDs at various gadolinium concentrations.

shown in Fig. 1(a), synthesized nanodroplets are relatively spherical in shape and have a mean size of 25.5 ± 4.1 nm in the TEM image. Dark contents in the NDs structure indicate loaded gadolinium ions within NDs.

UV-Vis experiments show that 92.11 ± 3.6% of the used drug has been entrapped into nanodroplets.

The stability assay for Gd-DOTA and doxorubicin-loaded nanodroplets was based on monitoring the size and drug encapsulation changes for 3 months. Any significant changes in size and drug encapsulation didn't observe during these 90 days as it is illustrated in Fig. 1 (b).

3.2. *In vitro passive drug release*

To evaluate whether NDs can regulate drug release, the DOX release models were assessed in phosphate buffer at pH values of 5.5 and 7.4. According to release kinetics (Fig. 2(a)) initially, the faster release rate of DOX was observed, it may be as a result of DOX settling on the NDs surface (Kumari et al., 2013; Liu et al., 2017). While a long-term release of DOX with slow diffusion, 68.99% up to 36 h, from alginate as a biopolymer matrix occurred. As Fig. 2(a) shows, the DOX is stabilized by the nanodroplet structure, so that its release was 20.4% at pH 7.4 after 12 h. However, the release of DOX from NDs at acidic pH (5.5, pH of endosomal/cytosomal environment) after 12 h was increased significantly (30.1%) (P-value < 0.05). These indicated that NDs is relatively pH-sensitive drug delivery system, although at natural pH (7.4) was firmly retained by the nanodroplets. In lower pHs, the greater release of DOX from NDs was occurred (Huang et al., 2017) because the hydrogen bonds strength between the DOX and the alginate can be reduced. It should be noted that pH-controlled DOX release of NDs in target therapy can facilitate local delivery of drugs by increasing their accumulation in tumor cells with pH acidic and as a result, the systemic side effects on the normal tissues around the tumor site was diminished (Hosseini et al., 2018; Kim et al., 2013).

3.3. *Ultrasound-induced drug release*

According to the active release profile, ultrasound exposure can trigger the release of 88.7% DOX from NDs within 10 min (Fig. 2 (b)). However, before US exposure drug was remained in the nanodroplets structure, and a little amount of DOX was released during 10 min (2.3%) from the NDs. The DOX molecules were stabilized with an alginate shell of phase-transition perfluorohexane nanodroplets. As a result of US exposure at adequately rarefactional pressures (Kripfgans et al., 2000), the perfluorohexane of NDs evaporated and turned into gas microbubbles. Undergo bubble implosion under the action of ultrasound, a massive amount of drug-loaded in NDs can be released. Controlled drug delivery system with smart drug release in the target site is one of the most important achievements in local cancer treatments.

3.4. *Magnetic properties of Gd-DOTA/DOX nanodroplets*

The magnetic properties of Gd-DOTA/DOX NDs were evaluated using a VSM with measuring magnetization (M) versus external

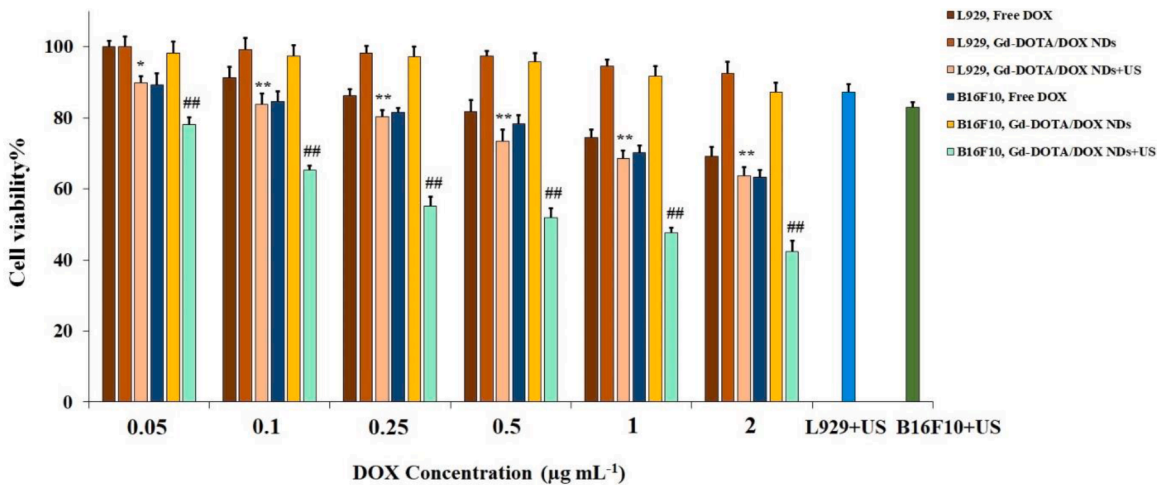

Fig. 6. Cytotoxicity results of ultrasound alone, free DOX, and Gd-DOTA/DOX NDs at different DOX concentrations against L929 normal and B16F10 cancer cells after 24 h incubation with and without sonication. Mean ± SD ($n = 3$). * P-value < 0.05 and ** P-value < 0.01, comparison with the non-sonication group for L929 cells. Compare with the non-sonication group for B16F10 cells, $^{\#}$ P-value< 0.05 and $^{\#\#}$ P-value< 0.01.

magnetic field (H) (Fig. 3). A linear relationship with a positive slope between two parameters of magnetization and the applied field proved the paramagnetic properties of Gd-DOTA and Gd-DOTA/DOX NDs (Dutta, 2015; Riyahi-Alam et al., 2015). The saturation magnetization (Ms) of Gd-DOTA was measured to be 0.61 emu g^{-1} (Fig. 3(a)), the Ms of the Gd-DOTA/DOX nanodroplets was 0.48 emu g^{-1} (Fig. 3(b)), less than for Gd-DOTA. These results showed that the alginate shell by encapsulating the Gd molecules reduced the saturation magnetization of the Gd. This decrease might be significantly attributed to the presence of nonmagnetic components such as alginate and DOX within the NDs (Zheng et al., 2018). But according to VSM curves (Fig. 3), the paramagnetic quality of the Gd compared to the Gd-DOTA has remained unchanged. These demonstrate the Gd-DOTA/DOX NDs with excellent paramagnetic behavior are promising candidates for MRI-guided drug delivery.

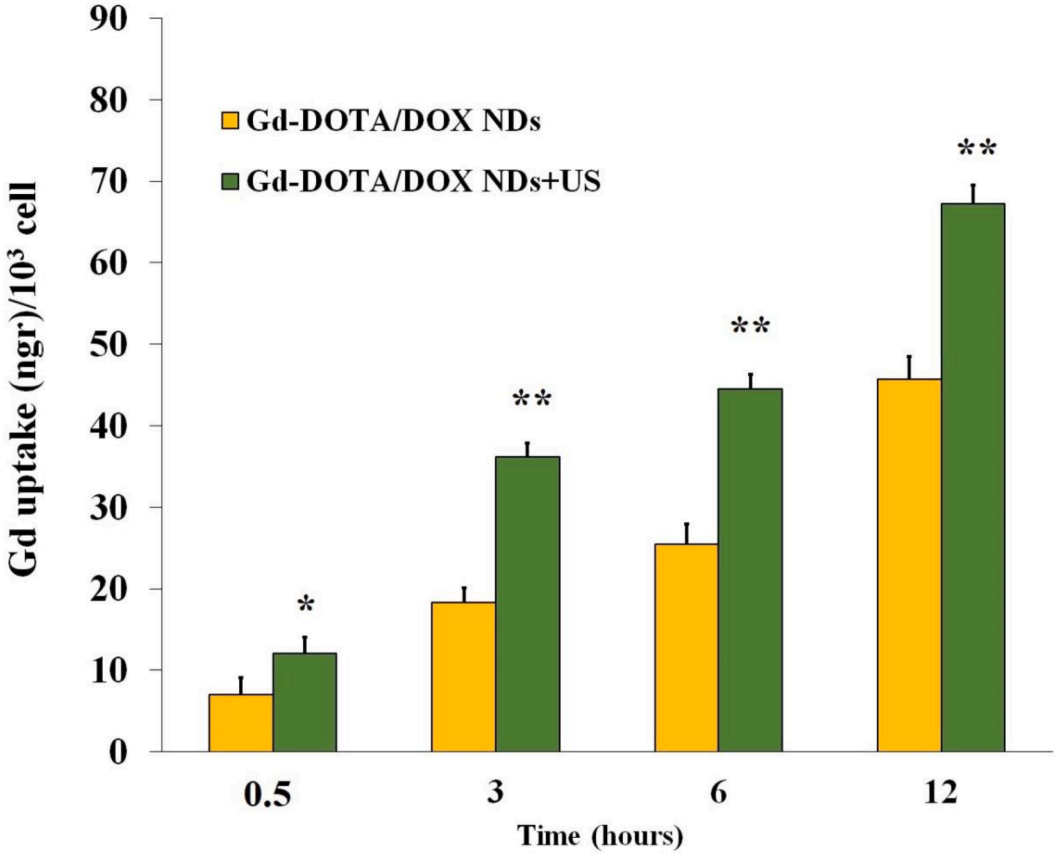

Fig. 7. Quantitative evaluation of cellular uptake of Gd-DOTA/DOX NDs (with and without sonication) by B16F10 cells after 0.5, 3, 6, and 12 h incubation by ICP-OES. Mean ± SD (n = 3). * P-value < 0.05 and ** P-value < 0.01, comparison with the non-sonication group.

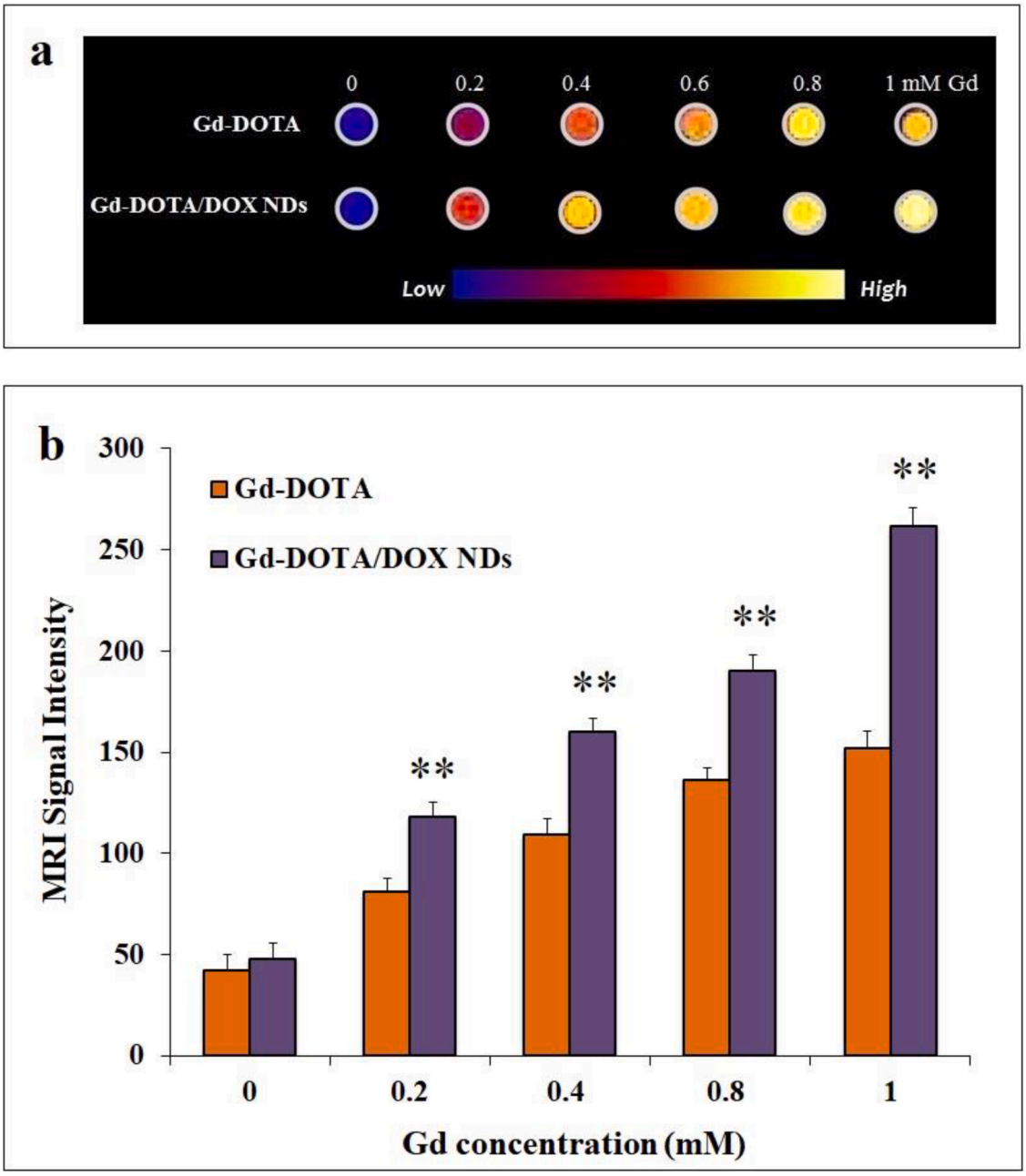

Fig. 8. (a) T_1-weighted MR images of Gd-DOTA and Gd-DOTA/DOX NDs in L929 and B16F10 cells at different concentrations of Gd^{+3} after 6 h incubation time. (b) Signal intensity analysis for MR images. Mean ± SD ($n = 3$). * P-value < 0.05 and ** P-value < 0.01, comparison with the control group. $^{\#}$ P-value < 0.05 and $^{\#\#}$ P-value < 0.01, comparison between the B16F10 and L929 cells treated with Gd-DOTA/DOX NDs.

3.5. Ultrasound imaging of Gd-DOTA/DOX NDs

For monitoring of acoustic droplet vaporization (ADV) effect, echogenic behavior of NDs, and formation of MBs from NDs were evaluated by diagnostic ultrasound imaging scanner (Fig. 4). The PBS control solution (Fig. 4(a)) showed a black image which indicates the lack of nano- and microbubbles. While, Fig. 4(b) showed the bright specks in the US image after NDs injection into PBS, demonstrating ultrasound-induced transition of NDs to MBs as a result of ADV effect. However, the temperature of the solution maintained constant at 37 °C during sonication, the NDs were converted to MBs under ultrasound exposure which confirmed the predominant effect of mechanical feature of US in inducing NDs vaporization. The ADV phenomenon and production of MBs could be promising for US imaging and controlled smart release drug delivery.

3.6. MRI relaxometry

Relaxometric measurements, as well as visualizing the contrasting properties of Gd-DOTA and nanocarriers containing Gd^{+3} (Gd-DOTA/DOX NDs) at varying concentrations was examined using a 1.5 T MRI clinical scanner. The MRI signal of both samples showed good dependence with gadolinium concentration, with a positive enhancement signal as the Gd concentration increased (Fig. 5 (a)). As the concentration of gadolinium increased, the color of MR images corresponding to SI changed from low to a high level. The T_1–relaxivity (r_1) of samples was obtained from the plotted relaxation rate ($R_1=1/T_1$) in terms of the gadolinium concentration graph. As shown in Fig. 5 (b), the R_1 showed a linear relationship with the Gd concentration. The r_1 value for Gd-DOTA/DOX NDs was calculated to be 6.34 $mM^{-1}s^{-1}$, which was higher than that of Gd-DOTA (4.52 $mM^{-1}s^{-1}$). The results suggested that

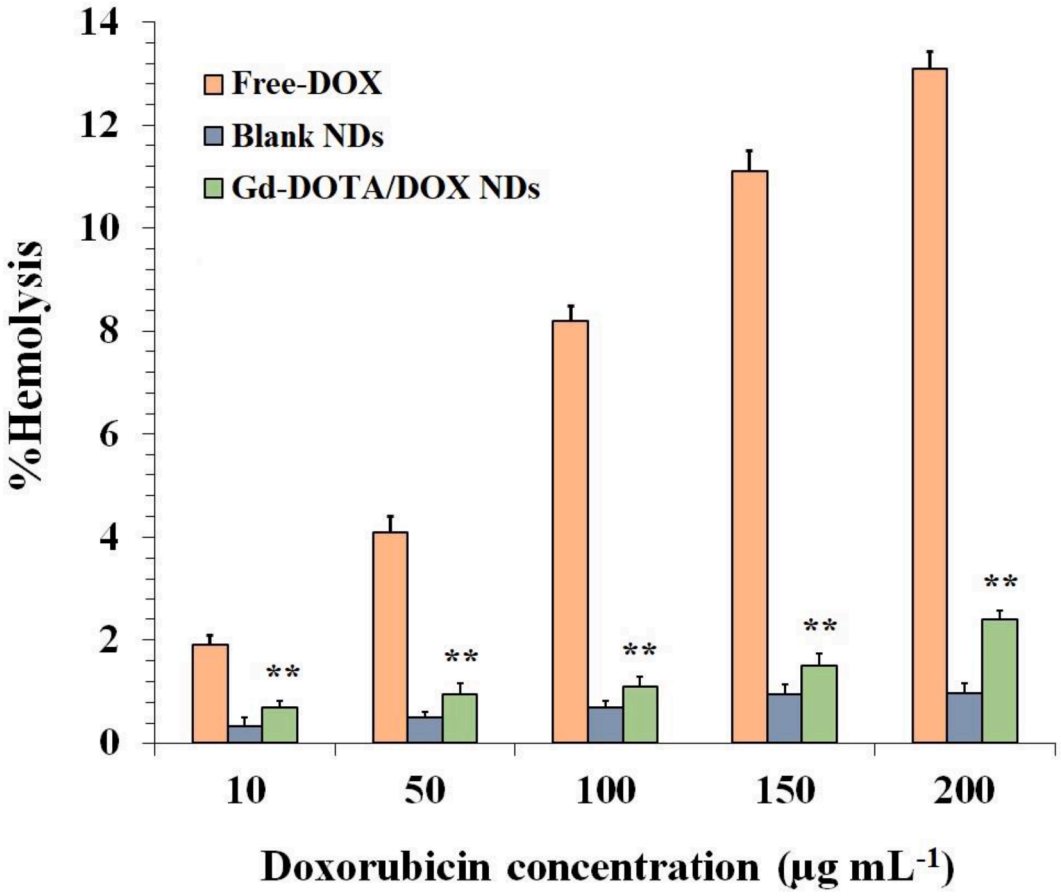

Fig. 9. Hemolytic activities of free DOX, blank NDs and Gd-DOTA/DOX NDs. Means ±SD ($n = 3$). Compare with the free-DOX group, * P-value< 0.05 and ** P-value< 0.01.

the Gd-DOTA/DOX NDs could be used as a positive contrast agent in T_1-weighted MR imaging.

3.7. In vitro cell viability study

Fig. 6 shows the results of MTT assay for ultrasound, free DOX and Gd-DOTA/DOX nanodroplets (with and without ultrasound exposure) against B16F10 and L929 cell lines after incubation for 24 h. Increases the NDs concentration resulted in enhanced cytotoxicity for both cell lines. Synthesized Gd-DOTA/DOX NDs showed no clear cytotoxic effect in different concentrations on both cell lines in comparison with control groups (P-value> 0.05), revealing their biocompatibility. However, cytotoxicity of nanodroplets against B16F10 cancer cells was higher than that of L929 normal cells at the same concentration (about 87.28 % cell viability for the B16F10 compared to about 92.64% for L929 at the concentration of 2 μgr mL^{-1} (P-value< 0.05)). This could be due to the higher uptake of Gd-DOTA/DOX NDs, resulted from the membrane of these cells, it causes more nanoparticles to be accumulated in these cells compared with the normal cells, resulting in more toxicity. The cytotoxicity of free DOX after loading into NDs significantly decreased for both cell lines (P-value<0.05). In addition, MTT assay results demonstrated higher cytotoxicity of NDs in combination with ultrasound compared to NDs and ultrasound alone group on cancer cells (P-value< 0.05) so that at 2 μg mL^{-1} concentration, ultrasound increased cytotoxicity of NDs about 45.3 % for B16F10 cells. This could be attributed to ultrasound-triggered DOX release under ADV effect and occurrence of cavitation that enhances the permeability of NDs and results in their more internalization into cancer cells (Ho and Yeh, 2017). The results demonstrated that Gd-DOTA/DOX NDs had little cytotoxicity and desirable biocompatibility. Therefore, synthesized nanoparticles have good potential to be used as a promising medical agent in biological applications such as controlled release drug delivery.

3.8. Cellular uptake

The ICP-OES assay was used to evaluate the intercellular uptake of NDs with and without sonication by melanoma cancer cells at different times. As Fig. 7 illustrates, the intracellular uptake of NDs increases as the NDs incubation time increases and reaches the highest value for 12 h incubation. Sonicated NDs (Gd-DOTA/DOX-NDs+US) had higher cellular uptake compared to non-sonicated NDs for all incubation times, which demonstrated the facilitated entering of NDs into the cancer cells through strong US mechanical effects including microstreaming and cavitation (Rapoport, 2012). In other words, the ultrasound waves can enhance the cells membrane permeability that causes entrance a lot of Gd ions to the cells. The data of ICP-OES analysis corroborate the MRI results which confirmed the capability of Gd-DOTA/DOX NDs to use as a nano-contrast agent for specific MRI of cancer cells.

3.9. Enhanced MR imaging, in vitro assay

The *in vitro* MRI on B16F10 cancer cells was obtained for evaluation of the Gd-loaded NDs ability in cancer cell imaging. For this purpose, the B16F10 cells were treated with Gd-DOTA and Gd-DOTA/DOX nanodroplets for 4 h and then scanned by the 1.5 Tesla MRI system. As shown in Fig. 8(a), the Gd-DOTA/DOX NDs treated group showed higher MRI signal enhancement comparison to the groups treated with Gd-DOTA. Besides, the signal intensity of the Gd-DOTA/DOX NDs group was 1.7-fold higher than that of the Gd-DOTA group at the 1 mM Gd concentration (Fig. 8(b)), indicating that the Gd-DOTA/DOX NDs have a higher

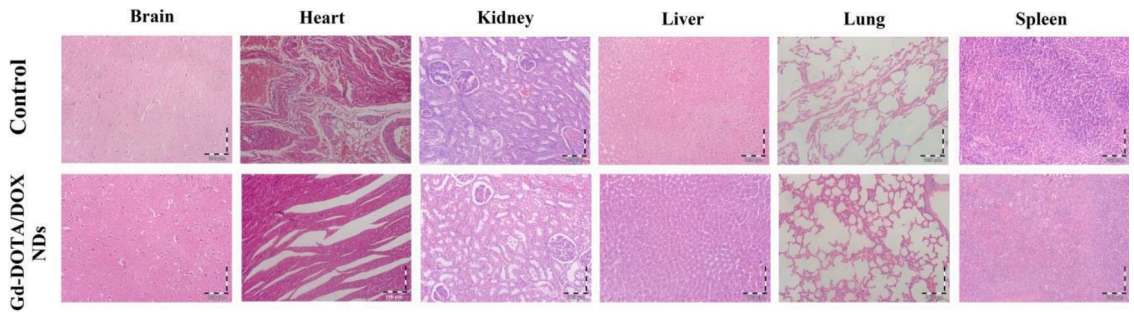

Fig. 10. Histological sections of different organs of normal mice, 3 weeks after PBS injection (control), and Gd-DOTA/DOX NDs.

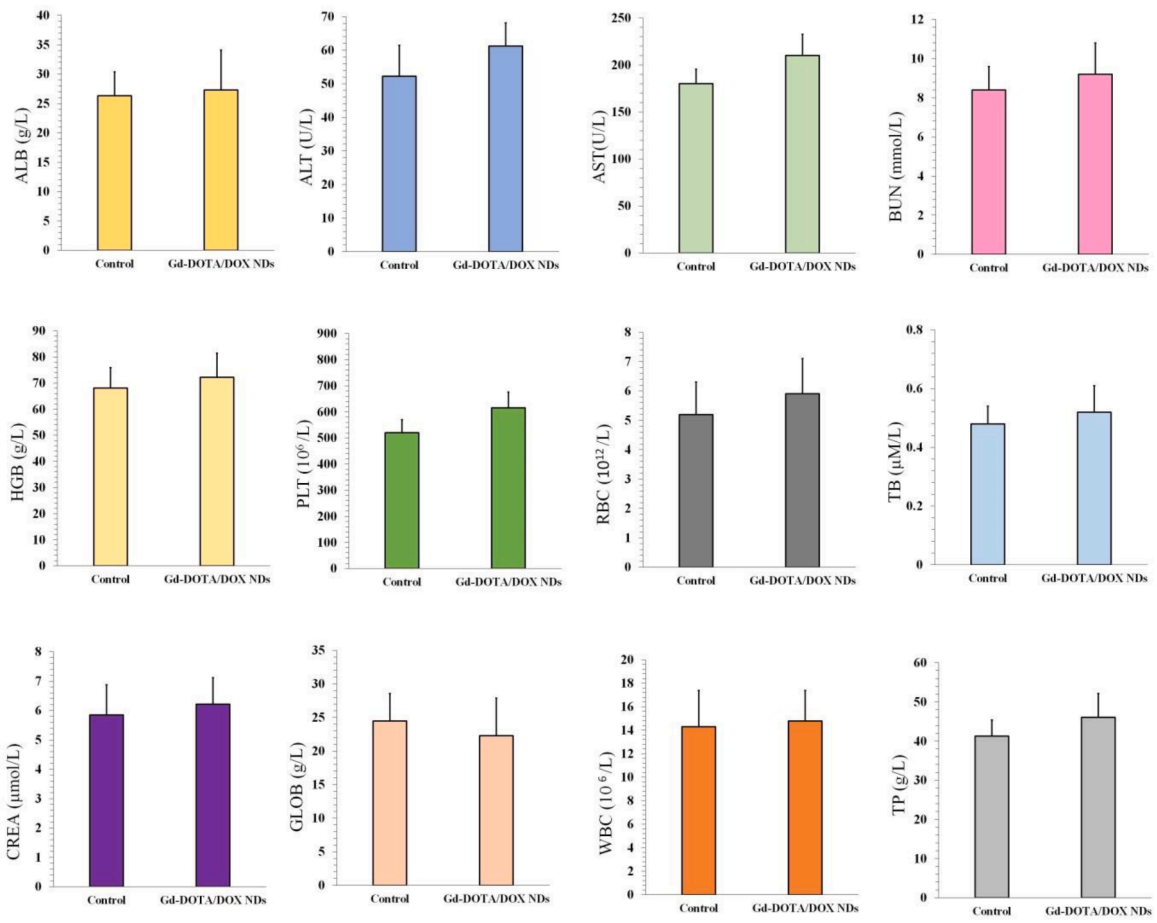

Fig. 11. Hematology analyze and blood biochemistry of the normal mice treated with PBS (control), and Gd-DOTA/DOX NDs.

contrast ability in T_1-weighted MR imaging. The results indicated that the Gd-DOTA/DOX NDs could use as an MRI contrast agent for cancer imaging and improve the relaxivity of the clinical product.

3.10. Hemolysis assay

Blood compatibility of nanoparticles that shows their biosafety on erythrocytes can be evaluate by hemolysis analysis (Shahbazi et al., 2013). The nanoparticles injected into blood vessel should have no adverse interaction with blood constituents. Fig. 9 shows the hemolytic activity of all samples especially DOX depended on their concentrations. The hemolysis of Gd-DOTA/DOX NDs was reached to the maximum level (13.1%) at 200 μg mL^{-1} DOX concentration. The hemolysis percentage in free DOX (13.1 %) and nanodroplets containing DOX (2.4 %) at 200 μg mL^{-1} showed significant differences. Doxorubicin accumulation by increasing the pressure of crystal osmotic in the RBCs that causes more water absorption, and finally the cell membrane rupture (Lu et al., 2010). DOX-loaded nanodroplets revealed negligible hemolytic activity in the studied concentration range. This could be contributed to hard penetration of NDs into red blood cells membrane as a result of their larger size in comparison to the DOX molecules. Unlike, alginate as a coating layer of nanodroplets led to the hemocompatibility of DOX. The hemolytic activity of blank nanodroplets was less than 1.5 %, indicating their high blood compatibility. The results suggested that Gd-DOTA/DOX nanodroplets are suitable for blood-contacting applications and intravenous administration.

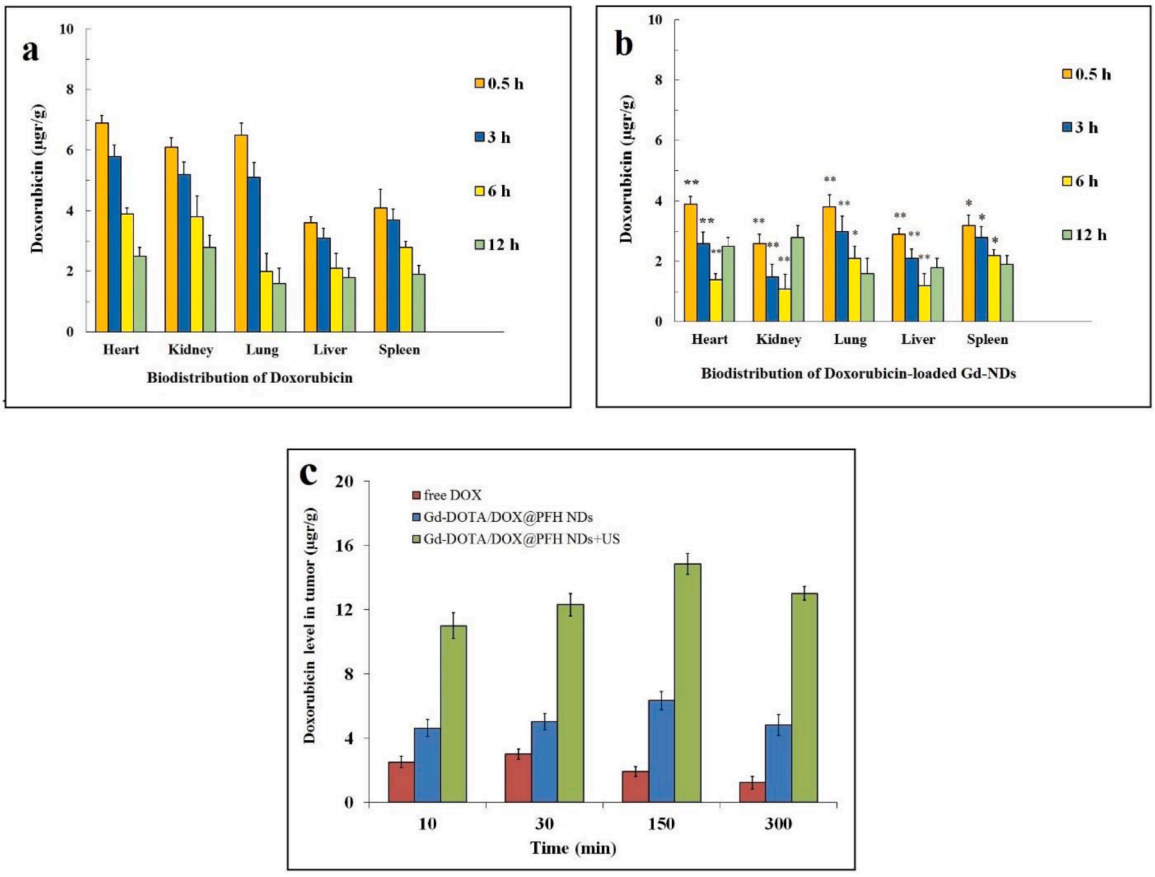

Fig. 12. Biodistribution profiles of (a) free DOX and (b) Gd-DOTA/DOX NDs in vital organs of mice, Means ± SD ($n = 3$). Compare with the free-DOX group, * P-value< 0.05 and ** P-value< 0.01 (c) DOX concentration in the tumor for DOX, Gd-DOTA/DOX NDs and Gd-DOTA/DOX NDs+US groups at different times after intravenous injection. Means ± SD ($n = 3$). Compare with the free-DOX group, $^{\#}$ P-value< 0.05 and $^{\#\#}$ P-value< 0.01.

3.11. Blood biochemical and histological assays

Toxicity is a great concern for nanoparticle-based drug carriers and the side effects usually limit their utilization for preclinical and clinical applications. The normal mice were injected with Gd-DOTA/DOX nanodroplets (2 mg kg^{-1} i.v) and they were sacrificed after 20 days to measure the nanodroplets biotoxicity. To biochemistry analysis and hematological assay (Fig. 11), the blood of mice was collected and their vital organs were harvested for the histopathological exam (Fig. 10). No significant changes were observed in concentrations of RBC, WBC, PLT, HGB, Cr, BUN, AST, ALT, TP, TB, GLOB, and ALB in either of the control and treated groups. In addition, the heart, kidneys, liver, brain, lungs, and spleen exhibited no organ damage compared to control groups and microscopic evaluations of all organs were normal. The results confirmed the high biocompatibility of synthesized nanodroplets, which makes them a promising candidate for theranostic applications.

3.12. In vivo biodistribution of DOX and Gd-DOTA/DOX nanodroplets

For *in vivo* biodistribution analysis, free DOX, and Gd-DOTA/DOX nanodroplets were injected to the tumor-bearing C57BL/6 mice and tumor region was exposed to ultrasound waves. The concentrations of DOX in vital organs and tumor were measured at different times after injection (Fig. 12). The DOX concentration for Gd-DOTA/DOX nanodroplets in different organs such as heart and kidneys was extremely lower than free DOX. For example, DOX concentration in heart for free DOX and Gd-DOTA/DOX nanodroplets at 3h post injection was 5.8 and 2.6 μg/g, respectively. Also, DOX concentration in kidneys for free DOX and Gd-DOTA/DOX nanodroplets at 3h post injection was 5.2 and 1.5 μg/g, respectively which are statistically significant. This could be attributed to biocompatible alginate that increases the biosafety of Gd-DOTA/DOX-loaded NDs. Therefore, encapsulating DOX in NDs decreases the nephrotoxicity and cardiotoxicity effects of DOX which are the main side effects of DOX (Guo et al., 2013; Lu et al., 2009; van Lummel et al., 2010; Xiong et al., 2006). Fig. 12 (c) shows DOX concentration in the tumor region at different times after injection. First, the DOX concentration for Gd-DOTA/DOX-loaded NDs in the tumor region was increased with a time-dependent trend and reached the maximum value of 150 min after injection.

The EPR effect allows conventional nanoparticles to accumulate and concentrate at tumor sites. When nanoparticles are delivered, they can be stored and released, and they can also be metabolized or eliminated gradually. A stable nanoparticle supply and enough delivery time lead to a dynamic balance of nanoparticle concentration between tissue systems and the blood. Two main clearance systems for nanoparticles *in vivo* are known. One system is the reticuloendothelial phagocytic system (RES) or mononuclear phagocytic system (MPS). Clearance and retention of nanoparticles are performed by this system. The macrophages phagocytose the nanoparticles and, after digestion, gradually excretes them into the blood and lead to permanent or temporary loss of the injected dose. The kidney and liver are the other clearance systems that are responsible for removing nanoparticles. These two organs play a major role in the removal of nanoparticles from the body (Wei et al., 2018; Yu and Zheng, 2015). In our previous study, the accumulation of nanodroplets in the tumor region and their elimination over time were investigated in *in vivo* MRI imaging (Maghsoudinia et al., 2021).

After 300 min, DOX concentration in the tumor region was decreased to about 4.82% for Gd-DOTA/DOX NDs and 13.02% for Gd-DOTA/DOX NDs+US. While free DOX reached the maximum value at 0.5 h after injection, and then it was decreased rapidly after that. In other words,

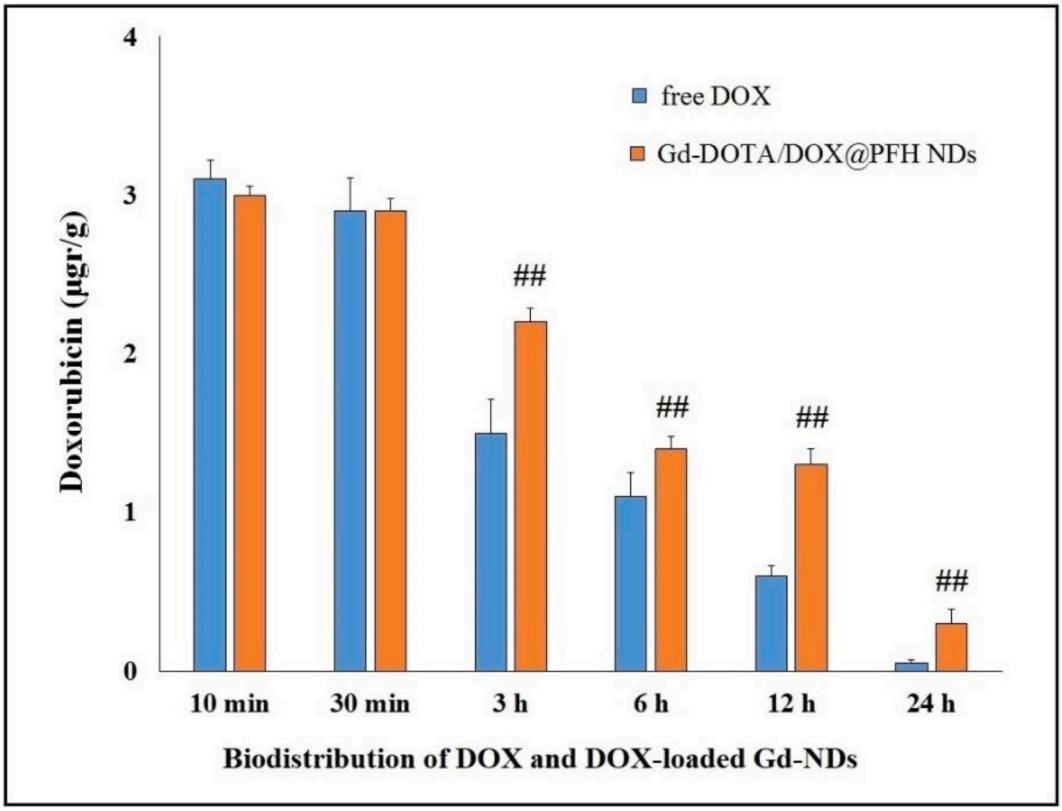

Fig. 13. The biodistribution of free DOX and Gd-DOTA/DOX NDs in blood of the mice.

Table 1
DOX pharmacokinetic parameters in mouse serum after IV injection of free DOX and DOX-loaded NDs.

PK Parameters	Free DOX	DOX-loaded NDs
K_{el} (h^{-1})	0.16	0.09
V_d (ml)	648.93	671.82
$t_{1/2}$ (h)	4.17	7.59
Cl (ml/h)	107.60	61.88

Kel first-order elimination rate constant; Vd volume of distribution; t1/2, elimination half –life; Cl, clearance

free DOX showed a more unstable accumulation profile compared to the Gd-DOTA/DOX NDs so that the concentration of DOX in the tumor region for nanodroplets group after 300 min was significantly higher than the free DOX group (P-value< 0.05). The lymphatic drainage of tumor is slower than normal tissues. It can be attributed to the interstitial and physiological properties of the tumor which causes more extravasation of macromolecules to the intercellular spaces. In addition, the tumor cells using enhanced permeability and retention (EPR) effects shows abnormal leakage to the macromolecules (Iyer et al., 2006).

3.13. Blood circulation time

As shown in Fig. 13, the two groups showed almost identical DOX concentration in blood after 10 and 30 min. It may be related to the sample preparation. In the process of sample preparation and extraction of DOX from blood, all available drug (DOX released from nanoparticles along with residual DOX in nanoparticles) were measured. Thus at the beginning of the drug concentration measuring, because the dose injected in the two groups was 2 DOX mg/kg, the same drug concentrations in two groups were measured, but over time, changes in the concentration of the drug happened. Pharmacokinetic evaluation illustrated an increased half-life of DOX and so increased concentrations of DOX in the nanoparticle group. Similar results were reported by Ghassami et al. (Ghassami et al., 2018). In addition, 24 h post injection, the concentration of DOX in the blood for free DOX group was very low and undetectable (0.05 µg/g), while for DOX-loaded NDs group was 0.3 µg/g. This indicated that the NDs had a longer blood circulation time. Therefore, NDs had a better chance of accumulating in the tumor cells. Besides, according to the passive drug release study, DOX was tightly remained to alginate shell of NDs in blood during the circulation and caused lower biotoxicity in comparison to free DOX.

In the differential equation, the rate of absorption and elimination of drugs relates to changes in drug concentration in the blood with time: If the variation of the concentration of drugs with time is linear, the rate equation is zero-order kinetics. But if the variation of the log concentration of drugs with time is linear, the rate equation is Frist-order kinetics. The results indicated that the distribution phase of DOX is one-compartment model (supplementary). In one-compartment model, the drug rapidly equilibrates with the tissue compartment. DOX pharmacokinetic parameters in mouse serum after IV injection of free DOX and DOX-loaded NDs were obtained (Table 1). Equations and graphs (Fig.S1) are available in supplementary.

4. Conclusion

The theranostic agents combining diagnostic and therapy properties for early detection of cancer and high-efficiency treatment have been gaining more and more attention in recent years. In this study, the Gd-DOTA/ DOX-loaded nanodroplet with ultrasound-triggered phase transition was introduced. In these NDs, Gd as a magnetic resonance contrast agent and doxorubicin as a chemotherapeutic drug demonstrated the usefulness of theranostic agents. Results of the present investigation indicated that Gd-DOTA/DOX NDs significantly increase MRI signal intensity ($r_1 = 6.34\ mM^{-1}S^{-1}$). Ultrasound images confirmed that nanodroplets can turn into microbubbles by acoustic droplet vaporization phenomenon which triggers encapsulated drug release and

showed strong ultrasound contrast. In conclusion, the favorable properties of synthesized nanodroplets including small size, high stability, MRI-guided and ultrasound controlled drug release ability, and excellent *in vivo* and *in vitro* biocompatibility confirmed that Gd-DOTA/DOX@PFH NDs can act as promising US/MRI-guided drug delivery nanocarriers to enhance chemoradiotherapy efficacy on melanoma cancer cells.

CRediT authorship contribution statement

Fatemeh Maghsoudinia: Visualization, Investigation, Writing – original draft, Investigation. **Hadi Akbari-Zadeh:** Software, Writing – review & editing, Investigation. **Fahimeh Aminolroayaei:** Software, Writing – review & editing. **Fariba Farhadi Birgani:** Software. **Ahmad Shanei:** Supervision, Project administration, Funding acquisition. **Roghayeh Kamran Samani:** Visualization, Supervision, Project administration, Writing – review & editing.

Acknowledgments

This manuscript is a part of a research project supported by Isfahan University of Medical Sciences by scientific code 198331.

Supplementary materials

Supplementary material associated with this article can be found, in the online version, at doi:10.1016/j.ejps.2022.106207.

References

Bhowmik, D., Gopinath, H., Kumar, B.P., Duraivel, S., Kumar, K.P.S., 2012. Controlled release drug delivery systems. Pharma. Innov. 1, 1–10.
Carvalho, C., Santos, R.X., Cardoso, S., Correia, S., Oliveira, P.J., Santos, M.S., Moreira, P.I., 2009. Doxorubicin: the good, the bad and the ugly effect. Curr. Med. Chem. 16, 3267–3285.
Chiari-Andréo, B.G., Abucafy, M.P., Manaia, E.B., da Silva, B.L., Rissi, N.C., Oshiro-Junior, J.A., Chiavacci, L.A., 2020. Drug delivery using theranostics: an Overview of its use, advantages and safety assessment. Curr. Nanosci. 16, 3–14.
Dutta, R., 2015. The applicability of rare earth gadolinium oxide nanoparticles for biomedical applications. Nanosci. Technol. Open Access. 2, 1–6.
Fasano, A., De Vloo, P., Llinas, M., Hlasny, E., Kucharczyk, W., Hamani, C., Lozano, A.M., 2018. Magnetic resonance imaging-guided focused ultrasound thalamotomy in parkinson tremor: reoperation after benefit decay. Mov. Disord. 33 (5), 848–849.
Franco, Y.L., Vaidya, T.R., Ait-Oudhia, S., 2018. Anticancer and cardio-protective effects of liposomal doxorubicin in the treatment of breast cancer. Breast Cancer Targets Ther. 10, 131.
Ghassami, E., Varshosaz, J., Jahanian-Najafabadi, A., Minaiyan, M., Rajabi, P., Hayati, E., 2018. Pharmacokinetics and *in vitro/in vivo* antitumor efficacy of aptamer-targeted Ecoflex® nanoparticles for docetaxel delivery in ovarian cancer. Int. J. Nanomed. 13, 493.
Guo, C., Sun, L., She, W., Li, N., Jiang, L., Luo, K., Gong, Q., Gu, Z., 2016. Dendronized heparin-gadolinium polymer self-assemble into nanoscale system as potential magnetic resonance imaging contrast agent. Polym. Chem. 7, 2531–2541.
Guo, H., Lai, Q., Wang, W., Wu, Y., Zhang, C., Liu, Y., Yuan, Z., 2013. Functional alginate nanoparticles for efficient intracellular release of doxorubicin and hepatoma carcinoma cell targeting therapy. Int. J. Pharm. 451 (1–2), 1–11.
Ho, Y.J., Yeh, C.K., 2017. Theranostic performance of acoustic nanodroplet vaporization-generated bubbles in tumor intertissue. Theranostics 7, 1477–1488.
Hosseini, F., Hosseini, F., Jafari, S.M., Taheri, A., 2018. Bentonite nanoclay-based drug-delivery systems for treating melanoma. Clay Miner. 53, 53–63.
Huang, D., Zhang, X., Zhao, C., Fu, X., Zhang, W., Kong, W., Zhang, B., Zhao, Y., 2021. Ultrasound-responsive microfluidic microbubbles for combination tumor treatment. Adv. Ther. 4, 2100050.
Huang, Y.S., Lu, Y.J., Chen, J.P., 2017. Magnetic graphene oxide as a carrier for targeted delivery of chemotherapy drugs in cancer therapy. J. Magn. Magn. Mater. 427, 34–40.
Iyer, A.K., Khaled, G., Fang, J., Maeda, H., 2006. Exploiting the enhanced permeability and retention effect for tumor targeting. Drug Discov. Today 11, 812–818.
Jeyamogan, S., Khan, N.A., Siddiqui, R., 2021. Application and importance of theranostics in the diagnosis and treatment of cancer. Arch. Med. Res. 52, 131–142.
Kim, H.K., Lee, G.H., Chang, Y., 2018. Gadolinium as an MRI contrast agent. Future Med. Chem. 10, 639–661.
Kim, I., Byeon, H.J., Kim, T.H., Lee, E.S., Oh, K.T., Shin, B.S., Lee, K.C., Youn, Y.S., 2013. Doxorubicin-loaded porous PLGA microparticles with surface attached TRAIL for the inhalation treatment of metastatic lung cancer. Biomaterials 34, 6444–6453.
Kripfgans, O.D., Fowlkes, J.B., Miller, D.L., Eldevik, O.P., Carson, P.L., 2000. Acoustic droplet vaporization for therapeutic and diagnostic applications. Ultrasound Med. Biol. 26, 1177–1189.
Kumari, S.D.C., Tharani, C.B., Narayanan, N., Kumar, C.S., 2013. Formulation and characterization of methotrexate loaded sodium alginate chitosan nanoparticles. Indian J. Res. Pharm. Biotechnol. 1, 915.
Lazaro-Carrillo, A., Filice, M., Guillén, M.J., Amaro, R., Viñambres, M., Tabero, A., Paredes, K.O., Villanueva, A., Calvo, P., del Puerto Morales, M., Marciello, M., 2020. Tailor-made PEG coated iron oxide nanoparticles as contrast agents for long lasting magnetic resonance molecular imaging of solid cancers. Mater. Sci. Eng. C 107, 110262.
Liu, G., Li, D.C., Li, P.P., Li, R.R., Chen, S.Y., 2017. Nanoparticle methotrexate delivery system for the treatment of paediatric patients with inflammatory bowel disease. Biomed. Res. 28 (8), 8–20.
Loskutova, K., Grishenkov, D., Ghorbani, M., 2019. Review on acoustic droplet vaporization in ultrasound diagnostics and therapeutics. Biomed Res. Int. 2019, 1–20.
Lu, D., Liang, J., Fan, Y., Gu, Z., Zhang, X., 2010. *In Vivo* evaluation of a pH-sensitive pullulan–doxorubicin conjugate. Adv. Eng. Mater. 12, B496–B503.
Lu, D., Wen, X., Liang, J., Gu, Z., Zhang, X., Fan, Y., 2009. A pH-sensitive nano drug delivery system derived from pullulan/doxorubicin conjugate. J. Biomed. Mater. Res. B. Appl. Biomater. 89, 177–183.
Maghsoudinia, F., Tavakoli, M.B., Samani, R.K., Hejazi, S.H., Sobhani, T., Mehradnia, F., Mehrgardi, M.A., 2021. Folic acid-functionalized gadolinium-loaded phase transition nanodroplets for dual-modal ultrasound/magnetic resonance imaging of hepatocellular carcinoma. Talanta 228, 122245.
Palekar-Shanbhag, P., Jog, S.V, Chogale, M.M., Gaikwad, S.S., 2013. Theranostics for cancer therapy. Curr. Drug Deliv. 10, 357–362.
Pinelli, F., Perale, G., Rossi, F., 2020. Coating and functionalization strategies for nanogels and nanoparticles for selective drug delivery. Gels 6, 6.
Rammohan, N., Filicko, A., MacRenaris, K., Ho, D., Meade, T.J., 2016. Theranostic nanodiamond-gadolinium (III)-doxorubicin conjugates improve chemotherapy of cancer cells that can be monitored by magnetic resonance imaging. Int. J. Radiat. Oncol. Biol. Phys. 96, E589.
Ranga, A., Agarwal, Y., Garg, K.J., 2017. Gadolinium based contrast agents in current practice: risks of accumulation and toxicity in patients with normal renal function. Indian J. Radiol. Imaging 27, 141.
Rapoport, N., 2012. Phase-shift, stimuli-responsive perfluorocarbon nanodroplets for drug delivery to cancer. Wiley Interdiscip. Rev. Nanomed. Nanobiotechnol. 4, 492–510. https://doi.org/10.1002/wnan.1176.
Riyahi-Alam, S., Haghgoo, S., Gorji, E., Riyahi-Alam, N., 2015. Size reproducibility of gadolinium oxide based nanomagnetic particles for cellular magnetic resonance imaging: effects of functionalization, chemisorption and reaction conditions. Iran. J. Pharm. Res. 14, 3–14.
Shafaei, E., Divband, B., Gharehaghaji, N., 2019. Relevance between MRI longitudinal relaxation rate and gadolinium concentration in Gd^{3+}/GO/alginate nanocomposite. Nanomed. J. 6, 263–268.
Shahbazi, M.-A., Hamidi, M., Mäkilä, E., Zhang, H., Vingadas Almeida, P., Kaasalainen, M., Salonen, J., Hirvonen, J., Santos, H., 2013. The mechanisms of surface chemistry effects of mesoporous silicon nanoparticles on immunotoxicity and biocompatibility. Biomaterials 34, 7776–7789.
Shanei, A., Akbari-Zadeh, H., Fakhimikabir, H., Attaran, N., 2019. The role of gold nanoparticles in sonosensitization of human cervical carcinoma cell line under ultrasound irradiation: an *in vitro* study. J. Nano Res. Trans. Tech. Publ. 59, 1–14.
Sheeran, P.S., Dayton, P.A., 2012. Phase-change contrast agents for imaging and therapy. Curr. Pharm. Des. 18, 2152–2165.
van Lummel, M., van Blitterswijk, W., Vink, S., Veldman, R., Valk, M., Schipper, D., Dicheva, B., Eggermont, A., ten Hagen, T., Verheij, M., Koning, G., 2010. Enriching lipid nanovesicles with short-chain glucosylceramide improves doxorubicin delivery and efficacy in solid tumors. FASEB J. 25, 280–289.
Wang, T.Y., Wilson, E, K Machtaler, S., K Willmann, J., 2013. Ultrasound and microbubble guided drug delivery: mechanistic understanding and clinical implications. Curr. Pharm. Biotechnol. 14, 743–752.
Wei, Y., Quan, L., Zhou, C., Zhan, Q., 2018. Factors relating to the biodistribution & clearance of nanoparticles & their effects on *in vivo* application. Nanomedicine 13, 1495–1512.
Xiao, Y.D., Paudel, R., Liu, J., Ma, C., Zhang, Z.S., Zhou, S.K., 2016. MRI contrast agents: classification and application. Int. J. Mol. Med. 38, 1319–1326.
Xiong, Y., Liu, X., Lee, C.P., Chua, B., Ho, Y.S., 2006. Attenuation of doxorubicin-induced contractile and mitochondrial dysfunction in mouse heart by cellular glutathione peroxidase. Free Radic. Biol. Med. 41, 46–55.
Yoon, H., Yarmoska, S.K., Hannah, A.S., Yoon, C., Hallam, K.A., Emelianov, S.Y., 2017. Contrast-enhanced ultrasound imaging *in vivo* with laser-activated nanodroplets. Med. Phys. 44, 3444–3449.
Yu, M., Zheng, J., 2015. Clearance pathways and tumor targeting of imaging nanoparticles. ACS Nano 9, 6655–6674.
Zheng, S., Han, J., Jin, Z., Kim, C.S., Park, S., Kim, K., Park, J.O., Choi, E., 2018. Dual tumor-targeted multifunctional magnetic hyaluronic acid micelles for enhanced MR imaging and combined photothermal-chemotherapy. Colloids Surf. B Biointerfaces 164, 424–435.
Zhu, J., Xiong, Z., Shen, M., Shi, X., 2015. Encapsulation of doxorubicin within multifunctional gadolinium-loaded dendrimer nanocomplexes for targeted theranostics of cancer cells. RSC Adv. 5, 30286–30296.